07,10,13

The dependencies of the melting point of Au, Pt and Fe on the nanocrystal size and shape at different pressures

© M.N. Magomedov

Institute for geothermal problems and renewable energy —
branch of the joint Institute of high temperatures of the Russian Academy of Sciences,
Makhachkala, Russia

E-mail: mahmag4@mail.ru

Received October 25, 2023
Revised October 25, 2023
Accepted December 27, 2023

A method is proposed for calculating the dependence of the melting temperature on the size (number of atoms N) and the nanocrystal surface shape at the different pressures (P). This method is based on the paired Mie–Lennard-Jones interatomic interaction potential, and takes into account the dependence of both the state equation and other lattice properties on the nanocrystal size and shape. For the first time, the dependences of the melting temperature (T_m) on the pressure P, size N, and shape parameter f of the nanocrystal were obtained. Calculations have been performed for gold, platinum and iron. It is shown that at any pressure, the $T_m(P, N, f)$ function decreases both with an isomorphic-isobaric (f, P — const) decrease in the number of N atoms, and with an isomeric-isobaric (N, P — const) deviation of the nanocrystal shape from the energy-optimal shape. It is shown that the value of the baric derivative of the melting temperature $T_m'(P)$ for a nanocrystal at low pressures is larger and at high pressures smaller than the value $T_m'(P)$ for a macrocrystal. Moreover, the dependence of the $T_m'(P)$ function on the nanocrystal size is negligible, i.e., the functions $T_m(P, \infty)$ and $T_m(P, N, f)$ are almost parallel at constant $N-f$-arguments. It is indicated how this method can be applied to experimentally estimate the pressure under which a nanocrystal is confined in a refractory matrix.

Keywords: nanocrystal, melting point, state equation, gold, platinum, iron.

DOI: 10.61011/PSS.2024.02.57919.241

1. Introduction

In recent years, it was experimentally shown that size effects have a significant impact on the baric dependences of various properties of nanocrystals [1–5]. Meanwhile, the theoretical size changes in baric dependences were studied very little. For example, until now no one studied (neither analytically nor by computer simulation) the change in the baric dependence of the melting point with decrease in nanocrystal size. This is due to the fact that the formulas for calculating the properties of nanocrystal of N atoms include the specific (per unit area) surface energy (σ), which depends on the specific (per atom) volume ($v = V/N$), temperature (T), size (or number of atoms N) and shape of the nanocrystal surface. However, the dependence of the function σ on the specific volume $v(T)$ turned out to be very difficult for determination both analytically and using computer simulation [6–10]. At the same time, without the dependence $\sigma(T, v, N)$ it is impossible to obtain the equation of state of the nanocrystal $P(T, v, N)$. That is why it was not yet possible to theoretically study the change in baric dependences of properties with nanocrystal size decreasing along various isotherms.

In this regard, in this paper the equation of state $P(T, v, N)$ and the baric dependences of lattice properties for nanocrystals of gold, platinum and iron were calculated by analytical method (i.e. without computer simulation) based on the pair potential of interatomic interaction. Based on these dependences, the change in the baric dependence of the melting point of gold, platinum and iron during the transition from macro- to nanocrystal with a certain surface shape was studied for the first time.

2. Method for calculating the properties of macro- and nanocrystals

The equation of state, thermoelastic and surface properties of gold macrocrystal were calculated in our paper [11] by the method, which is based on the paired 4-parameter interatomic interaction potential of Mie–Lennard-Jones, which has the following form:

$$\varphi(r) = \frac{D}{(b-a)}\left[a\left(\frac{r_o}{r}\right)^b - b\left(\frac{r_o}{r}\right)^a\right], \qquad (1)$$

where D and r_o — depth and coordinate of the potential minimum, $b > a > 1$ — numerical parameters.

In the paper [12], based on the method from [11] and the delocalization criterion for the phase transition crystal–liquid, the expression was obtained for calculating the baric dependence of the melting point (T_m) for a single-

component macrocrystal, which has the form

$$T_m(P) = T_m\big(P, T_m(0)\big) \times \exp\left[-\frac{b}{3}\alpha_P\big(P, T_m(0)\big)\big[T_m\big(P, T_m(0)\big) - T_m(0)\big]\right], \quad (2)$$

where $T_m(0)$ — melting point of macrocrystal at $P = 0$, $\alpha_p\big(P, T_m(0)\big)$ — coefficient of thermal volumetric expansion at pressure P, calculated along the isotherm $T_m(0)$ [11,12],

$$T_m\big(P, T_m(0)\big) = T_m(0)\left[\frac{c_o\big(P, T_m(0)\big)\Theta_o\big(P, T_m(0)\big)}{c_o\big(0, T_m(0)\big)\Theta_o\big(0, T_m(0)\big)}\right]^2 \times \frac{f_y\big(y_w(P, T_m(0))\big)}{f_y\big(y_w(0, T_m(0))\big)}. \quad (3)$$

Here $c_o = (6k_p v/\pi)^{1/3}$ — the distance between the centers of the nearest atoms in a vacancy-free lattice (this is indicated by the index „o“), k_p — structure packing factor, Θ_o — Debye temperature for vacancy-free lattice [11]:

$$\Theta_o(k_n^o, c_o) = A_w(k_n^o, c_o)\xi\left[-1+\left(1+\frac{8D}{k_B A_w(k_n^o, c_o)\xi^2}\right)^{1/2}\right], \quad (4)$$

where k_n^o — the first coordination number in vacancy-free lattice, k_B — Boltzmann constant, the function $A_w(k_n^o, c_o)$ arises from consideration of the energy of „zero vibrations“ of atoms in system

$$A_w(k_n^o, c_o) = K_R\frac{5k_n^o ab(b+1)}{144(b-a)}\left(\frac{r_o}{c_o}\right)^{b+2}, \quad (5)$$

$$K_R = \frac{\hbar^2}{k_B r_o^2 m}, \quad \xi = \frac{9}{k_n^o(N=\infty)}.$$

Here $\hbar$ — Planck's constant, m — atomic mass.

Function $f_y(y_w)$ is included in (3) in order to consider quantum effects and is written as

$$f_y(y_w) = \frac{2}{y_w}\frac{[1-\exp(-y_w)]}{[1+\exp(-y_w)]}, \quad y_w = \frac{3\Theta_o}{4T}. \quad (6)$$

Based on the potential (1), within the „only nearest neighbors interaction“ approximation, the following expression may be derived for the equation of state and isothermal modulus of elasticity (B_T) [11]:

$$P = \left[\frac{k_n^o}{6}DU'(R) + \frac{9}{4}k_B\Theta_o\gamma_o E_w(y_w)\right]\frac{1}{v}, \quad (7)$$

$$B_T = -v\left(\frac{\partial P}{\partial v}\right)_T = P + \left[\frac{k_n^o}{18}DU''(R) + \frac{9}{4}k_B\Theta_o\gamma_o(\gamma_o - q_o)E_w(y_w) - 3k_B\gamma_o^2 T F_E(y_w)\right]\frac{1}{v}. \quad (8)$$

Here, $R = r_o/c_o = (v_0/v)^{1/3}$ is the relative linear density of the system,

$$E_w(y_w) = 0.5 + \frac{1}{[\exp(y_w)-1]},$$

$$F_E(y_w) = \frac{y_w^2\exp(y_w)}{[\exp(y_w)-1]^2},$$

$$v_0 = \frac{\pi r_o^3}{6k_p}, \quad U(R) = \frac{aR^b - bR^a}{b-a}, \quad (9)$$

$$U'(R) = R\left[\frac{\partial U(R)}{\partial R}\right] = \frac{ab(R^b - R^a)}{b-a},$$

$$U''(R) = R\left[\frac{\partial U'(R)}{\partial R}\right] = \frac{ab(bR^b - aR^a)}{b-a}.$$

Expressions for the first (γ_o) and second (q_o) Gruneisen parameters for the vacancy-free crystal that are included in (7) and (8) can be derived from (4). They are written as follows

$$\gamma_o = -\left(\frac{\partial\ln\Theta_o}{\partial\ln v}\right)_T = \frac{b+2}{6(1+X_w)}, \quad (10)$$

$$q_o = \left(\frac{\partial\ln\gamma_o}{\partial\ln v}\right)_T = \gamma_o\frac{X_w(1+2X_w)}{(1+X_w)}.$$

Here, function $X_w = A_w\xi/\Theta_o$ is introduced, which determines the role of quantum effects in calculating the Gruneisen parameters.

Since, according to (4), the Debye temperature does not change with emperature during isochoric heating of the system, the isochoric heat capacity and isobaric coefficient of thermal volumetric expansion for the vacancy-free crystal can be determined as follows [11]:

$$C_v = 3Nk_B F_E\left(\frac{3\Theta_o}{4T}\right),$$

$$\alpha_p = \frac{1}{v}\left(\frac{\partial v}{\partial T}\right)_P = \gamma_o\frac{C_v}{VB_T} = \frac{\gamma_o C_v}{NB_T[\pi r_o^3/(6k_p)]}\left(\frac{v_0}{v}\right). \quad (11)$$

Expressions (4)–(11) allowed us in [11] to determine the equation of state and the baric dependence of the lattice properties of gold macrocrystal, and also allowed us in [12] to calculate with using formulas (2) and (3) the baric dependence of the melting point of macrocrystals Au, Pt and Nb. In this paper the change in the baric dependence of the melting point of gold during the transition from macro- to nanocrystal was studied on the basis of the method from [12], which was summarized for nanocrystal of N atoms. This summarization was made on the basis of the RP-model, the essence of which is as follows [13,14]. Limiting the system to a surface leads to the breaking of bonds at the boundary. Therefore, if „only nearest neighbors interaction“ approximation is used, then instead of the first coordination number $k_n^o(\infty)$ it is necessary to use $k_n^o(N, f)$ — average (over the entire nanosystem) value of the first coordination number, which will depend on both the size and shape of the nanosystem. In this case, the packing index of the system structure (k_p) is assumed to be unchanged: $k_p = \text{const}$. Let us assume that nanocrystal with free Gibbs surface has the form of a rectangular parallelepiped with a square base, faceted with (100) type faces. The value $f = N_{ps}/N_{po}$ is a shape

parameter, which is determined by the ratio of the number of atoms on the side edge N_{ps} to the number of atoms on the base edge N_{po}. For a rod-like shape $f > 1$, for a cube $f = 1$, for a plate-shaped nanocrystal $f < 1$. The number of atoms in nanocrystal is equal to: $N = fN_{po}^3/\alpha$, varies within: $2^3/\alpha \le N \le \infty$, where $\alpha = \pi/(6k_p)$ — structure parameter. Within the RP model, the dependence of the normalized average value of the first coordination number on the size (N) and shape (f) of the nanocrystal has the form [13,14]:

$$k_n^{o*} = \frac{k_n^o(N, f)}{k_n^o(\infty)} = 1 - Z_s(f)\left(\frac{\alpha^2}{N}\right)^{1/3}, \qquad (12)$$

where $k_n^o(\infty) = k_n^o(N = \infty)$ — the first coordination number for the macrocrystal,

$$Z_s(f) = \frac{1 + 2f}{3f^{2/3}}.$$

The shape function $Z_s(f)$ reaches a minimum equal to 1 at $f = 1$, i.e. for the cube shape. For plate ($f < 1$) or rod-like ($f > 1$) forms, the value of $Z_s(f)$ is greater than 1. Therefore, the function $k_n^o(f)^*$ at any N has a maximum at $f = 1$, i.e. for the most energetically optimal cubic shape of rectangular parallelepiped. This model of nanocrystal in the form of the rectangular parallelepiped, the shape of which can be varied using the shape parameter f, was called the RP-model.

The volume and surface area for the RP-model are equal to [13,14]:

$$V = N_{po}^3 f c_o^3 = N\alpha c_o^3,$$

$$\Sigma = 6c_o^2(N\alpha^2)^{2/3} Z_s(f),$$

here it can be seen that the volume of the nanocrystal V does not depend on the shape of the system, i.e. on the value f.

The functions from (4)−(11) are determined by the parameters of the interatomic potential (1) and the following arguments: T, v, k_n^o, k_p. Therefore, using the dependence $k_n^o(N, f)$ from (12) at $k_p = \text{const}$, we can summarize the formulas from (4)−(11) for the case of nanocrystal of N atoms, which has the form of rectangular parallelepiped, the shape of which is determined by the shape parameter f. As was shown in [13–18], this method made it possible to study the dependence of various properties of nanocrystal on both the size and its shape under various $P-T$-conditions.

Within RP model the baric dependence of the melting point from (2) can be summarized for the case of nanocrystal of N atoms in the form

$$T_m(P, N) = T_m\big(P, T_m(0), N\big) \exp\Bigg[-\frac{b}{3}\alpha_p\big(P, T_m(0), N\big) \times \big[T_m\big(P, T_m(0), N\big) - T_m\big(0, T_m(0), N\big)\big]\Bigg], \qquad (13)$$

Here we introduce functions that summarize (3) for the case of nanocrystal

$$T_m\big(P, T_m(0), N\big) = T_m\big(0, T_m(0), N\big) \times \left[\frac{c_o\big(P, T_m(0), N\big)\Theta_o\big(P, T_m(0), N\big)}{c_o\big(0, T_m(0), N\big)\Theta_o\big(0, T_m(0), N\big)}\right]^2 \times \frac{f_y\big(y_w(P, T_m(0), N)\big)}{f_y\big(y_w(0, T_m(0), N)\big)}. \qquad (14)$$

$$T_m\big(0, T_m(0), N\big) = T_m(0) \times \left[\frac{c_o\big(0, T_m(0), N\big)\Theta_o\big(0, T_m(0), N\big)}{c_o\big(0, T_m(0), \infty\big)\Theta_o\big(0, T_m(0), \infty\big)}\right]^2 \times \frac{f_y\big(y_w(0, T_m(0), N)\big)}{f_y\big(y_w(0, T_m(0), \infty)\big)}. \qquad (15)$$

In „thermodynamic limit“ (i.e. when $N \to \infty$ and $V \to \infty$ at $v = V/N = \text{const}$) from (12) we obtain $k_n^{o*}(N \to \infty) = 1$, from (15) we obtain $T_m(0, T_m(0), N \to \infty) = T_m(0)$, and (14) goes into function (3).

For almost all metals the energy of a pair interatomic bond is much greater than the energy of „zero vibrations“ of atoms, i.e., the condition is satisfied

$$\frac{8D}{k_B A_w(k_n^o, c_0)\xi^2} \gg 1.$$

Then formula (4) can be simplified to form

$$\Theta_o(k_n^o, c_o) \cong \left[\frac{8DA_w(k_n^o, c_o)}{k_B}\right]^{1/2} = \left[\frac{5\hbar^2 D k_n^o a b(b+1)}{18k_B^2 m r_o^2 (b-a)}\left(\frac{r_o}{c_o}\right)^{b+2}\right]^{1/2}. \qquad (16)$$

Using (16) the ratio can be easily obtained

$$[c_o(P, T, N)\Theta_o(P, T, N)]^2 \cong \frac{5\hbar^2 D k_n^o(N) a b(b+1)}{18k_B^2 m(b-a)} \times \left(\frac{r_o}{c_o(P, T, N)}\right)^b. \qquad (17)$$

At high temperatures (i.e. at $T \gg \Theta_o$) the function $f_y(y_w)$ is close to 1: $f_y(y_w \ll 1) \cong 1$. Therefore, the ratio of these functions in (14) and (15) may be assumed equal to 1. Then formula (14) and (15) can be simplified to form

$$T_m\big(P, T_m(0), N\big) \cong T_m(0) k_n^{o*}(N)\left[\frac{c_o\big(0, T_m(0), \infty\big)}{c_o\big(P, T_m(0), N\big)}\right]^b, \qquad (18)$$

$$T_m\big(0, T_m(0), N\big) \cong T_m(0) k_n^{o*}(N)\left[\frac{c_o\big(0, T_m(0), \infty\big)}{c_o\big(0, T_m(0), N\big)}\right]^b. \qquad (19)$$

From (13), (18) and (19) it is clear that the change in the baric dependence of the melting point with nanocrystal size decreasing is determined by three functions

$$k_n^o(N, f), \quad c_o(P, T, N, f), \quad \alpha_p(P, T, N, f).$$

3. Calculation results for gold

Gold (Au, atomic mass $m(\mathrm{Au}) = 196.967$ a.m.u.) is a poorly oxidized, inert and ductile metal. Gold has a face-centered cubic (FCC) structure ($k_n^o(\infty) = 12$, $k_p = 0.7405$, $\alpha = \pi/(6k_p) = 0.70709$) and does not undergo any polymorphic phase transitions up to 220 GPa [19]. That is why the equation of state and baric dependences of the properties of FCC-Au macrocrystal are well studied and it is used as a pressure standard [20]. It is also often used to study the size dependences of various properties [6,21].

For FCC-Au the parameters of the pair interatomic potential (1) were determined by us by the self-consistency method in [22], and they have the following values:

$$r_o = 2.87 \cdot 10^{-10}\,\mathrm{m}, \quad D/k_B = 7446.04\,\mathrm{K},$$

$$b = 15.75, \quad a = 2.79. \qquad (20)$$

FCC-Au macrocrystal has a melting point equal to: $T_m(P = 0, N = \infty) = 1337$ K [23]. For the macrocrystal the equation of state and baric dependences of the lattice properties pg FCC-Au with the parameters of the interatomic potential (20) were calculated by us using the method from (2)–(11) in [11,12]. The baric dependences obtained in [11,12] for FCC-Au macrocrystal showed good agreement with the experimental and theoretical results of other authors. Therefore, in this paper we used the potential parameters from (20).

In this paper we studied the change in baric dependences during the transition from macrocrystal to nanocrystal of $N = 306$ atoms. The value of $N = 306$ atoms was chosen for the following reasons. On the one hand, we wanted to illustrate most vividly the difference in baric dependences for macro- and nanosized systems. However, on the other hand, as was shown experimentally in [24–28], and also by computer simulation in [29,30], and by the analytical method in [31–34], with the decrease in size of nanoparticle (nanocrystal or nanodroplet) with free surface, the parameters of the phase transition crystal–liquid (PT C–L) in it change. Moreover, at a certain number of atoms (N_0) the specific (per atom) latent heat of PT C–L disappears: $\Delta h(N_0) = 0$, and jump in specific volume of FP C–L: $\Delta v(N_0) = 0$. Thus, at $N \le N_0$ the phase difference disappears, and PT C–L is no longer possible here, since for such a cluster the thermodynamic concept of the solid or liquid phase is no longer applicable. For $P = 0$ the following estimates were theoretically obtained: for metals $N_0 = 300$ [29], and 50–300 [32]; for silicon: $N_0 = 23$–400 [33]. For FCC-argon it was shown by the analytical method in [34] that S-loop of PT C–L on the isotherm of the equation of state disappears at the following cluster sizes: $N_0(T = 150\,\mathrm{K}) = 485$ (i.e. $N_{po} = 7$) and $N_0(T = 60\,\mathrm{K}) = 38$ (i.e. $N_{po} = 3$).

Besides, we took the value $N = 306$ to study the influence of the nanocrystal shape on both the equation of state and the baric dependences of the lattice properties. The main calculations were made for nanocrystal of $N = fN_{po}^3/\alpha = 306$ atoms with the energetically optimal shape of rectangular parallelepiped, i.e., with the shape of cube: $f = 1$, $N_{po} = 6$, $k_n^* = 0.882152$, $k_n = 10.5858$. However, some of the calculations were made for nanocrystal of $N = fN_{po}^3/\alpha = 306$ atoms, but in the form of rod, i.e. at $f = 8$, $N_{po} = 3$, $N_{ps} = N_{po} f = 24$, $k_n^* = 0.833048$, $k_n = 9.99658$. This provided an opportunity to examine the variation of properties with an isothermal-isobaric change in the nanocrystal shape.

3.1. Equation of state

The change in the function $c_o(P, T, N, f)$ is determined by change in the equation of state $P(v, T, N, f)$. Figure 1, *a* shows the behavior of the equation of state of FCC-Au, i.e. the isothermal dependences of the pressure (P, in GPa) on normalized volume ($v/v_0 = (c_o/r_o)^3 = R^{-3}$) along three isotherms (bottom-up): 100, 300, 1337 K. Figure 1, *B* shows the baric dependence for the isochoric derivative $(\partial P/\partial T)_v$ (in 10^{-3} GPa/K), which was calculated by formula [35]:

$$\left(\frac{\partial P}{\partial T}\right)_v = \alpha_p B_T.$$

Solid thick curves show the results for macrocrystal, i.e. for $N = \infty$. The dotted lines show the results for cubic nanocrystal of $N = 306$ atoms at $f = 1$. The thin solid line for 1337 K shows the result for rod-shaped nanocrystal of $N = 306$ atoms at $f = 8$. The asterisk in Figure 1, *B* shows the result of calculating the value of $\alpha_p B_T$ for the FCC-Au macrocrystal at $P = 0$ and $T = 300$ K [36].

From Figure 1, *A* it is clear that upon transition from macro- to nanocrystal, the pressure rise decreases with decrease in the specific volume. This indicates decrease in the modulus of elasticity: $B_T = -v(\partial P/\partial v)_T$, with decrease in nanocrystal size. The function B_T decreasing with decrease in the nanocrystal size was obtained both theoretically and experimentally in papers of other authors [5,37–41]. Calculations showed that at isomer-isothermal (N, T — const) deviation of the nanocrystal shape from the energy-optimal shape (for RP-model this is cube) the slope of the function $P(v/v_o)$ decreases. This means that at isomerically–isotherm–isochoric deformation of the cubic nanocrystal its modulus of elasticity decreases.

It is evident from Figure 1, *A* that isothermal dependences $P(v/v_0)$ for nano- and macrocrystals intersect at a certain value of relative volume $(v/v_0)_0$. Thus, at a point with coordinates: $(v/v_0)_0, P_0$, surface pressure becomes zero: $P_{Sf}(T, N)_0 = P(T, \infty)_0 - P(T, N)_0 = 0$. At $P > P_0$ the surface pressure compresses the nanocrystal ($P_{Sf} > 0$); and

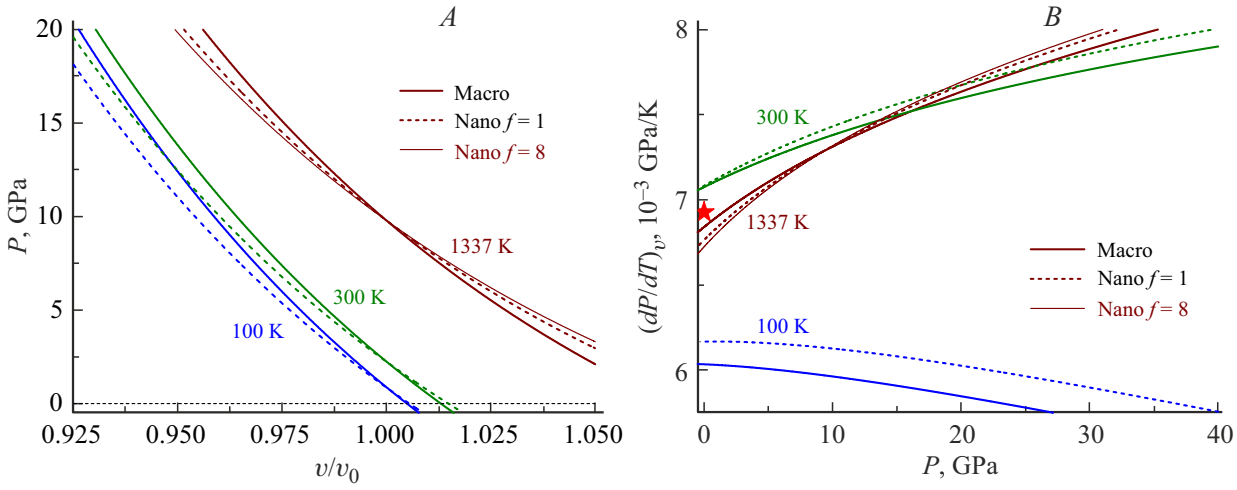

Figure 1. Isotherms of the equation of state (A) and baric dependence for the isochoric derivative $(\partial P/\partial T)_v$ (B). Solid curves — calculations for the macrocrystal. Dashed lines — results for cubic nanocrystal. The thin solid line for 1337 K represents the result for a rod-shaped nanocrystal. The asterisk in Figure 1, B shows the result from [36] for macro-Au at $P = 0$ and $T = 300$ K.

at $P < P_0$ the surface pressure stretches the nanocrystal: $P_{Sf} < 0$. The value $(v/v_0)_0$ decreases (i.e. P_0 increases) both at isomorphic-isomeric (f, N — const) increase in temperature, and at isomorphic–isothermal (f, T — const) N decreasing.

Note that in addition to our papers [13,14,22], a negative value of surface pressure in nanocrystal was also obtained in the papers of other authors who used the analytical calculation method: for FCC-Au in [15], for BCC-Nb in [16], for BCC-W in [17], for BCC of substitutional alloy Mo–W in [18]. In the paper [42] the surface pressure for spherical FCC-Ag nanocrystal was studied using molecular dynamics simulations. In [42] the transition of nanocrystal surface pressure to the negative region was also indicated. The stretching of Sr nanocrystal was also obtained in [43]. In the paper [37] it was experimentally shown that as the size of diamond nanocrystal decreases at $P = 0$ its density decreases. In the paper [44] it was experimentally shown that as the size of FCC ruthenium (FCC-Ru) nanocrystal decreases at $P = 0$, the average interatomic distance in it increases. These results also indicate that the nanocrystal is stretched by surface pressure.

As can be seen from Figure 1, B at low temperatures $T < 100$ K the function $(\partial P/\partial T)_v$ increases both with isomorphic-isobaric decrease in the number of atoms N, and with isomeric–isobaric deviation of the nanocrystal shape from the energy-optimal shape (for RP-model this is cube). However, for $T > 300$ K, the function $(\partial P/\partial T)_v$ depends weakly on the size and shape of the nanocrystal. In [11] it was shown that there is a certain temperature T_B, in the region of which the Birch approximation is satisfied, which assumes that at high temperatures the product $\alpha_p B_T$ does not depend on pressure. In [11] for FCC-Au macrocrystal it was obtained: $T_B(N = \infty) = 137 \pm 15$ K. In this paper, for FCC-Au nanocrystal of cubic form consisting of $N = 306$ atoms, the following was obtained: $T_B(N = 306) = 131 \pm 15$ K.

3.2. Thermal expansion coefficient

The thermal expansion coefficient — is parameter that at $P = 0$ is measured with very high accuracy [45]. However, the baric dependence of the function α_p is very difficult to measure. Figure 2 shows the baric (A) and temperature (B) dependences of the thermal expansion coefficient (α_p, 10^{-6} 1/K) for FCC-Au. Baric dependences were calculated along three isotherms (from bottom to top): 100, 300, 1337 K. Temperature dependences are calculated along three isobars (from top to bottom): 0, 24, 60 GPa. Solid thick curves show the results for macrocrystal, dotted lines show the results for cubic nanocrystal of $N = 306$ atoms. The thin solid line for 1337 K shows the result for rod-shaped nanocrystal of $N = 306$ atoms. The asterisks in Figure 2 show the results of calculations at $P = 0$ from [36]. In Figure 2, B solid circles show experimental data for FCC-Au macrocrystal from the paper [45]. The dashed line, which merges with our solid line, shows the theoretical isobaric ($P = 24$ GPa) dependence $\alpha_p(T)$ for FCC-Au from [46].

From Figure 2 it is clear that the value α_p increases during the transition from macro- to nanocrystal under any P–T-conditions, and the size increase in the function α_p is greater the greater the shape of the nanocrystal deviates from the energy-optimal shape (for RP-model this is cube). However, the difference $\alpha_p(N)-\alpha_p(\infty)$ decreases with isomorphic–isomeric–isothermal increase in pressure. This is due to the fact that at high pressure the difference between the vibration amplitudes for atom on the surface and for atom in the bulk of nanocrystal decreases. Therefore, with pressure increasing the role of surface atoms in the size increase in the function $\alpha_p(T)$ decreases.

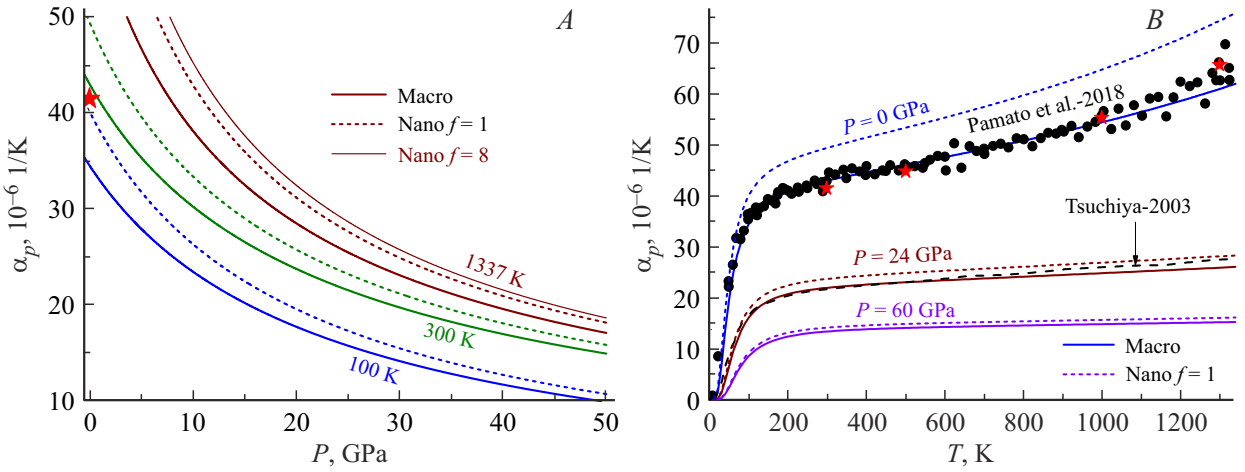

Figure 2. Baric (A) and temperature (B) dependences of the thermal expansion coefficient for FCC-Au. Solid curves — calculations for macrocrystal, dotted lines — calculations for cubic nanocrystal. The thin solid line for 1337 K represents the result for a rod-shaped nanocrystal.

Note that increase in the function α_p upon transition from macro- to nanocrystal at $P = 0$ was obtained in many papers (see, for example, [39,47]). As for the size change in the baric dependence of the function α_p, then existing experimental or theoretical methods yet did not made it possible to obtain such estimates even at $T = 300$ K. However, the dependence of functions α_p and $\alpha'_p(P)$ on the size of the nanocrystal under various $P-T$-conditions was studied within the RP-model by the analytical method for Si in [13], for substitution alloy Au–Fe in [14], for BCC-Nb in [16], for BCC-W in [17], for BCC substitution alloy Mo–W in [18].

3.3. Melting point

When using potential parameters (20), using formulas (5)–(11) for included in equations (14) and (15) parameters along isotherm $T_m(0) = 1337$ K at $P = 0$

$$c_o\big(0, T_m(0), \infty\big) = 2.93432 \cdot 10^{-10}\,\text{m},$$

$$\Theta_o\big(0, T_m(0), \infty\big) = 168.280\,\text{K},$$

$$c_o\big(0, T_m(0), 306, 1\big) = 2.94560 \cdot 10^{-10}\,\text{m},$$

$$\Theta_o\big(0, T_m(0), 306, 1\big) = 152.793\,\text{K},$$

$$c_o\big(0, T_m(0), 306, 8\big) = 2.95162 \cdot 10^{-10}\,\text{m},$$

$$\Theta_o\big(0, T_m(0), 306, 8\big) = 145.823\,\text{K}.$$

were obtained.

Using these values and formulas (2)–(15), the baric dependences of the melting point were calculated for both macro- and nanocrystals of 306 atoms with cubic and rod-shaped surfaces. Figure 3 shows baric dependences for the melting point $T_m(P)$ (left graph A), and for the melting point derivative with respect to pressure: $T'_m(P) = dT_m/dP$ (right graph B). Function $T'_m(P)$ was calculated by means of numerical differentiation of isothermal dependences from (13) with respect to pressure. In Figure 3 the solid and dashed lines show the experimental dependences for the FCC-Au macrocrystal from papers [48] and [23], respectively. These experimental data were approximated by the three-parameter Simon–Glatzel equation of the following form:

$$T_m(P) = T_{m0}\left[1 + \frac{P}{P_0}\right]^{c_s}, \tag{21}$$

$$T'_m(P) = \frac{dT_m(P)}{dP} = T_{m0}\frac{c_s}{P_0}\left[1 + \frac{P}{P_0}\right]^{c_s - 1}. \tag{22}$$

In the paper [48] for FCC-Au for the pressure range up to 6 GPa we obtained $T_{m0} = 1339$ K, $P_0 = 16.1$ GPa, $c_s = 0.57$ — solid line in Figure 3.

In the paper [23] for FCC-Au for the pressure range up to 106 GPa we obtained $T_{m0} = 1337$ K, $P_0 = 22.265 \pm 1.83$ GPa, $c_s = 0.662 \pm 0.03$ — dashed line in Figure 3.

Also in the paper [23] the dependence $T_m(P, \infty)$ for FCC-Au was calculated using the molecular dynamics simulations method. For the pressure range up to 107 GPa we obtained

$$T_{m0} = 1181\,\text{K}, \quad P_0 = 17.94\,\text{GPa}, \quad c_s = 0.709.$$

This calculated dependence is shown in Figure 3 by a dash-dotted line. Our calculation for macrocrystal is shown by solid thick line, which practically merges with the experimental dependence $T_m(P)$ from [23]. The dotted line shows our calculations for cubic nanocrystal of 306 atoms. The thin solid line shows our calculations for rod-shaped nanocrystal of 306 atoms.

As can be seen from Figure 3, A the dependence $T_m(P)$ for a nanocrystal lays below the dependence for macrocrystal. Moreover, the difference $T_m(P, \infty) - T_m(P, N)$

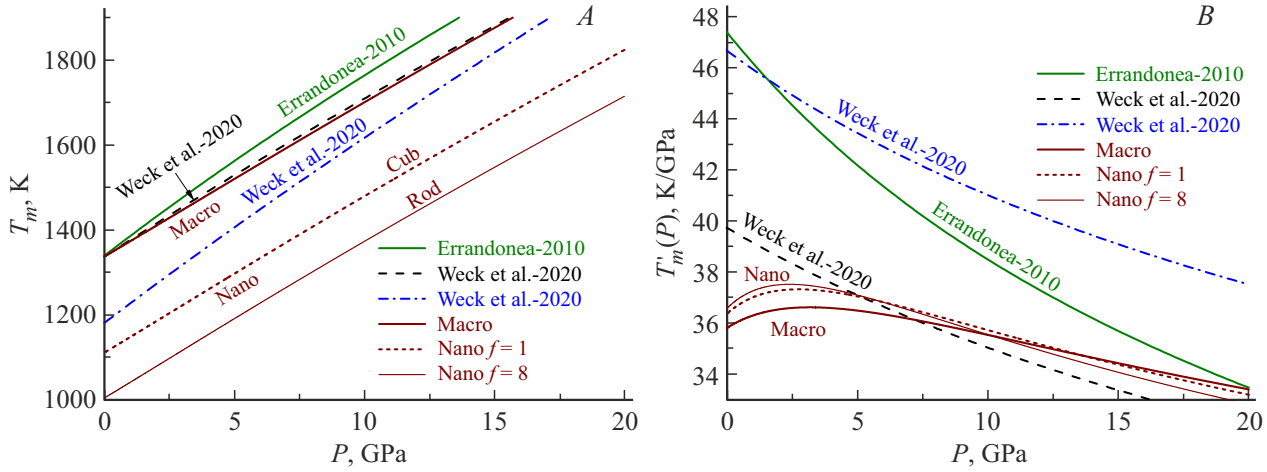

Figure 3. Baric dependence of the melting point (A) and its derivative with respect to pressure $T'_m(P)$ (B) for FCC-Au.

is greater, the greater the nanocrystal shape deviates from the energetically optimal shape (for the RP-model this is cube). This is consistent with the experimental and theoretical results obtained for FCC-Au at $P = 0$ in [15,21,29,32,41,49–53]. From Figure 3, B it also follows that during isobaric heating of an array of isomeric (i. e. with the same number of atoms N) nanocrystals the nanocrystals whose shape deviates most from the energetically optimal shape will melt first. Nanocrystals with energetically optimal shape have maximum melting point for a given number of atoms. This was first stated in the paper [54]. In this case, the shape relaxation can occur, i. e., nanocrystal with „non-optimal" shape, having melted, can immediately crystallize into a more „heat-resistant" energy-optimal shape.

As can be seen from Figure 3, B the baric dependences of the functions $T'_m(P)$ for cubic macro- and nanocrystal intersect at the point: $P_x = 13.63$ GPa, $T'_m(P)_x = 34.75$ K/GPa. This means that at low pressures the value $T'_m(P)$ increases, and at $P > P_x$ the value $T'_m(P)$ decreases upon isomorphic-isobaric decrease in the size of the nanocrystal. However, as can be seen from Figure 3, B, the dependence of the function $T'_m(P)$ on size and shape is insignificant. This indicates that with constant $N-f$ arguments the baric dependences $T_m(P, \infty)$ and $T_m(P, N, f)$ are practically parallel.

Note that the dependences of the melting point on size and shape at various pressures were also studied by the analytical method from (5)–(11) for Si in [13,33], for FCC-Au in [15], for BCC-Nb in [16], and for BCC-Mo in [49]. However, in these papers a simplified formula was used to calculate the dependence $T_m(P, N)$, which we described in detail in [12]. Therefore, the agreement with the experimental data for macrocrystal in these papers was worse than that obtained by us in Figure 3.

Today, experimental and theoretical determination of the dependence $T_m(N)$ even at $P = 0$ is a very difficult task [52,53]. Therefore, in the literature there are many different dependencies $T_m(P = 0, N)$, which lie in a wide range [15,52,53]. For example, according to estimates from [52, Figure 2], for a spherical Au nanoparticle with a radius of 1.1 nm (i. e. of $N = 309$ atoms) „surface melting temperature" lies in the range:

$$T_m(P = 0, N = 309)_{\text{surf}} = 200-600^\circ\text{C} = 473-873\,\text{K},$$

a „melting temperature of the core" of nanoparticles is by 200–250 K higher. Thus, the entire Au nanocrystal of 309 atoms will melt after 1073–1123 K. In our calculations for homogeneous nanocrystal with geometric Gibbs surface, we obtained (Figure 3, B):
for cubic shape:

$$T_m(P = 0, N = 306,\ f = 1) = 1111.34\,\text{K},$$

for rod shape:

$$T_m(P = 0, N = 306,\ f = 8) = 1004.58\,\text{K}.$$

When the method of calculating the dependence $T_m(P, N, f)$ was tested using gold, we decided to apply it to other metals. The dependences $T_m(P, N, f)$ were calculated for platinum and two polymorphs of iron similarly to gold.

4. Results of melting point calculation for platinum

Platinum (Pt, $m(\text{Pt}) = 195.084$ a.m.u.) has FCC structure (i. e. $k_n^o(\infty) = 12$, $k_p = 0.7405$, $\alpha = \pi/(6k_p) = 0.70709$) and does not experience polymorphic phase transitions up to 200 GPa [55–58]. Therefore, platinum, similarly to gold, is used as pressure standard [20]. However, the experimental data for dependence $T_m(P, \infty)$ from [55–58] is very inconsistent which is caused by the refractory property of this metal. At $P = 0$ the melting point of platinum macrocrystal is $T_m(0, \infty) = 2041.7$ K [57].

Pair interatomic potential parameters (1) for FCC-Pt were calculated by the self-consistency method in [22] according to the calculations using the equation of state,

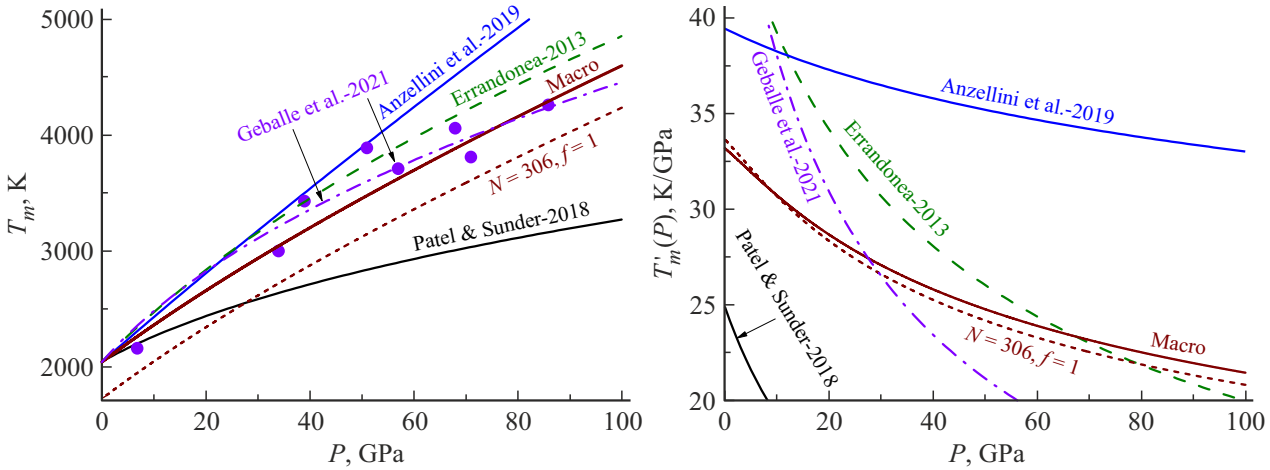

Figure 4. Baric dependence of the melting point (left) and its derivative with respect to pressure $T'_m(P)$ (right) for FCC-Pt. Our calculations for macro-Pt are shown by the central solid line, and for nano-Pt by the dotted line.

thermal expansion coefficient, modulus of elasticity and other properties of FCC-Pt macrocrystal. They are as follows:

$$r_o = 2.766 \cdot 10^{-10}\,\text{m}, \quad D/k_B = 11400.7\,\text{K},$$

$$b = 11.65, \quad a = 3.05. \tag{23}$$

For the FCC-Pt macrocrystal, we calculated the baric dependence of the melting point using the method from (2)–(11) with the interatomic potential parameters from (23) in [12]. $T_m(P, \infty)$ dependence obtained in [12] for FCC-Pt macrocrystal showed good agreement with the experimental results. Therefore, in this paper we used the potential parameters from (23) to study the properties of FCC-Pt nanocrystal consisting of $N = f\,N_{po}^3/\alpha = 306$ atoms with energetically optimal shape of rectangular parallelepiped, i.e., with cube shape: $f = 1$, $N_{po} = 6$, $k_n^* = 0.882152$, $k_n = 10.5858$.

When using potential parameters (23) using formulas (5)–(11) on the isotherm $T_m(0, \infty) = 2041.7\,\text{K}$ at $P = 0$ for parameters included in formulas (14) and (15) we obtained

$$c_o\big(0, T_m(0), \infty\big) = 2.82146 \cdot 10^{-10}\,\text{m},$$

$$\Theta_o\big(0, T_m(0), \infty\big) = 221.477\,\text{K},$$

$$c_o\big(0, T_m(0), 306, 1\big) = 2.83042 \cdot 10^{-10}\,\text{m},$$

$$\Theta_o\big(0, T_m(0), 306, 1\big) = 203.58\,\text{K}.$$

Using these values and formulas (2)–(15), the baric dependences of the melting point were calculated for both macro- and nanocrystal of 306 atoms with cubic shape of surface. Figure 4 shows baric dependences for the melting point $T_m(P)$ (left graph), and for the melting point derivative with respect to pressure: $T'_m(P) = dT_m/dP$ (right graph).

In Figure 4 various lines show the experimental dependences obtained in [55–58] for the FCC-Pt macrocrystal, and approximated by the three-parameter Simon–Glatzel equation (21) with parameters: $T_{m0} = 2042\,\text{K}$, $P_0 = 21.5\,\text{GPa}$, $c_s = 0.5$ — dashed line [55], $T_{m0} = 2041\,\text{K}$, $P_0 = 15.1\,\text{GPa}$, $c_s = 1/2.6 = 0.3846$ — dashed-dotted line [58], $T_{m0} = 2046\,\text{K}$, $P_0 = 23\,\text{GPa}$, $c_s = 0.28$ — bottom solid line [56],

The upper solid line in Figure 4 shows the calculated dependences (21) and (22), obtained in the paper [57] using the ab initio Z-method calculations, which were approximated by the dependence (21) with parameters: $T_{m0} = 2041.7\,\text{K}$, $P_0 = 44\,\text{GPa}$, $c_s = 0.85$ — upper solid line [57].

Solid circles show experimental data for $T_m(P)$ from [58].

Our calculations for macrocrystal are shown by the central solid thick line. The dotted line shows our calculations for cubic nanocrystal of 306 atoms.

As can be seen from Figure 4 the dependence $T_m(P)$ for nanocrystal lays below the dependence for macrocrystal. A decrease in the melting point with size decreasing of FCC-Pt nanocrystal at $P = 0$ was also obtained using the classical molecular dynamics computer simulations method for spherical nanocrystal of $1953 < N < 13500$ in [59], and of $1435 < N < 18140$ in [60].

The calculations showed that nanocrystals with energy-optimal shape have maximum melting point for a given number of atoms. The baric dependences of the functions $T'_m(P)$ for cubic macro- and nanocrystals have no maximum as in case of gold. The dependences $T'_m(P)$ for cubic macro- and nanocrystals intersect in point: $P_x = 8.87\,\text{GPa}$, $T'_m(P)_x = 31.00\,\text{K/GPa}$. This means that at low pressures the value $T'_m(P)$ increases, and at $P > P_x$ the value $T'_m(P)$ decreases upon isomorphic-isobaric decrease in the size of the nanocrystal. However, as in the case of gold, the dependence of the function $T'_m(P)$ on size and shape for FCC-Pt is insignificant. This indicates that with constant $N-f$ arguments the baric dependences $T_m(P, \infty)$ and $T_m(P, N, f)$ are practically parallel.

Parameters of the interatomic potential Mie−Lennard-Jones (1) for the BCC and FCC structures of iron from [22,70] and value $V_0 = [\pi N_A/(6k_p)]r_o^3$. (The right columns show the calculated at $P = 0$ and $T_m(0, \infty) = 1811$ K values of molar volume ($V = [\pi N_A/(6k_p)]c_o^3$), Debye temperature, Gruneisen first parameter, thermal expansion coefficient and modulus of elasticity. For each structure, the first line presents calculations for macrocrystal, and the second line shows calculations for cubic nanocrystal of $N = 281$ (for BCC) and 306 (for FCC) atoms)

Phase	r_o, 10^{-10} m	D/k_B, K	b	a	V_0, cm^3/mol	V, cm^3/mol	Θ, K	γ	α_p, 10^{-6} K^{-1}	B_T, GPa
BCC-Fe	2.4775	12561.53	8.37	3.09	7.0494	7.5968	372.61	1.7211	47.91	117.71
						7.6977	340.17	1.7217	58.06	95.93
FCC-Fe	2.5404	8374.353	8.37	3.09	6.9812	7.5233	363.42	1.7213	47.92	118.86
						7.6139	334.45	1.7218	57.10	98.64

5. Results of melting point calculation for iron

The dependence $T_m(P, \infty)$ for iron is studied for a long time [61–64], but this dependence still causes a lot of disputes [65–67]. Iron (Fe, m(Fe) = 55.847 a.m.u.) has several crystal modifications, as a result there are two triple points on the dependence $T_m(P, \infty)$ of iron. At low pressures, the paramagnetic phase δ-Fe with a body-centered cubic (BCC) structure is stable: $k_n^o(\infty) = 8$, $k_p = 0.6802$, $\alpha = \pi/(6k_p) = 0.769774$. At $P = 0$ the melting point of BCC-Fe macrocrystal is $T_m(0, \infty) = 1811$ K [61,62]. With pressure increasing in the dependence $T_m(P, \infty)$ of iron a triple point $\delta-\gamma$-liquid is observed with coordinates [61,62]:

$$P_{\delta-\gamma\text{-liquid}} = 5.2\,\text{GPa}, \quad T_{\delta-\gamma\text{-liquid}} = 1991\,\text{K}. \tag{24}$$

At this point, BCC-δ-Fe, FCC-γ-Fe and the liquid phase of iron coexist.

Upon further increase in pressure, the triple point $\gamma-\varepsilon$-liquid is observed with coordinates [65,66]:

$$P_{\gamma-\varepsilon\text{-liquid}} = 98.5\,\text{GPa}, \quad T_{\gamma-\varepsilon\text{-liquid}} = 3712\,\text{K}. \tag{25}$$

At this point FCC-γ-Fe, the liquid phase and phase ε-Fe with hexagonal structure coexist. Note that other coordinate values for these triple points are presented in the literature (see review in [65–67]), however, when calculating the dependence $T_m(P, N)$of iron we used data from (24) and (25).

The parameters of the pair interatomic potential Mie−Lennard-Jones (1) for BCC-Fe were determined by us by the self-consistency method in [22] based on calculations of the equation of state, the thermal expansion coefficient, the modulus of elasticity and other properties of the macrocrystal BCC-Fe. Potential parameters (1) for FCC-Fe were determined by us in [68] based on studying the phase transition BCC-FCC in iron. We tested these parameters when studying the substitution alloy Au−Fe in [14,69,70], as well as when studying the parameters of vacancy and self-diffusion formation in the BCC and FCC phases of iron in [71]. The values of the potential parameters (1) for the BCC and FCC phases of iron from [22,70], as well as the value of the molar volume $V_0 = [\pi N_A/(6k_p)]r_o^3$ are presented in the Table.

Here N_A — Avogadro's number. The right columns of Table show the calculated at $P = 0$ and $T_m(0, \infty) = 1811$ K values of molar volume ($V = [\pi N_A/(6k_p)]c_o^3$), Debye temperature, Gruneisen first parameter, thermal expansion coefficient and modulus of elasticity. The right columns for each structure in the first line present calculations for macrocrystal, and the second line shows calculations for cubic nanocrystal of $N = fN_{po}^3/\alpha$ atoms at $f = 1$ and $N_{po} = 6$. Thus, for nanocrystals with BCC and FCC structures, we obtained

$$N(\text{bcc}) = 281, \;\; k_n^* = 0.871704, \;\; k_n = 6.97364,$$

$$N(\text{fcc}) = 306, \;\; k_n^* = 0.882152, \;\; k_n = 10.5858.$$

Figure 5 shows the experimental and theoretical baric dependences of the melting point $T_m(P)$ (graphs A and C) and its derivative with respect to pressure $T_m'(P) = dT_m/dP$ (B and D) for BCC and FCC-Fe in the pressure range 0−20 GPa (A and B) and 0−100 GPa (C and D). The triple points $\delta-\gamma$-liquid and $\gamma-\varepsilon$-liquid with coordinates from (24) and (25) are shown as solid dots. The experimental dependence from [65] was approximated by the four-parameter Simon−Glatzel equation of the following form:

$$T_m(P) = T_m^*\left[1 + \frac{P - P^*}{P_0}\right]^{c_s}, \tag{26}$$

$$T_m'(P) = T_m^*\,\frac{c_s}{P_0}\left[1 + \frac{P - P^*}{P_0}\right]^{c_s - 1}. \tag{27}$$

For FCC-Fe the following parameters were obtained in the article [65]: $T_m^* = 1991$ K, $P^* = 5.2$ GPa, $P_0 = 27.39$ GPa, $c_s = 1/2.38 = 0.42$ — dashed line in Figure 5.

Recently, analytical methods for calculating the dependence $T_m(P, \infty)$ for an iron macrocrystal were proposed in papers [72,73]. In these papers the statistical moment method (SMM) was used, and the three-parameter Morse function was used as the pair interatomic potential [72,73]. In [72] the dependence $T_m(P, \infty)$ was calculated by the SMM method using the Lindemann criterion for macrocrystal of the hexagonal phase ε-Fe. By approximating the

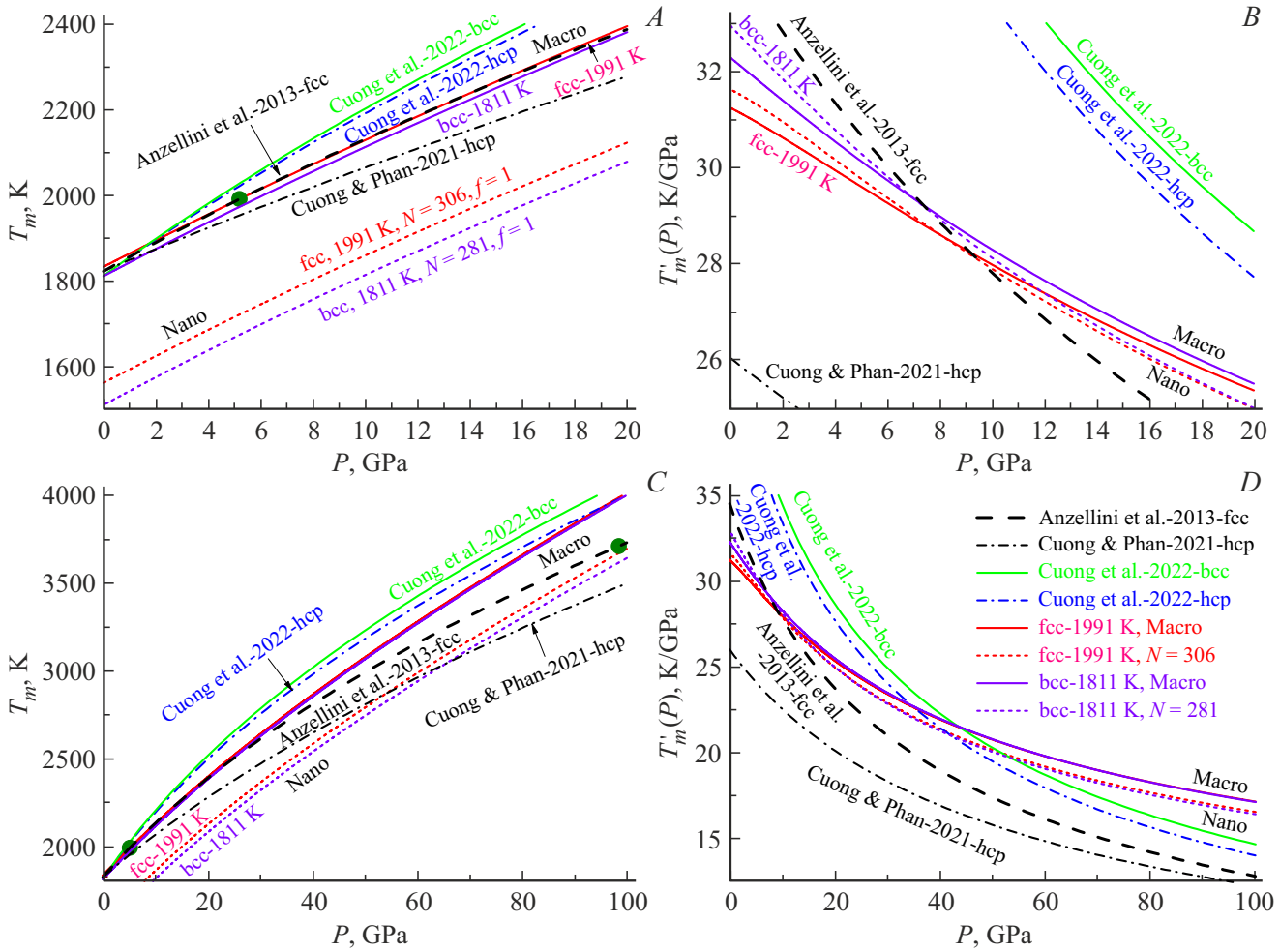

Figure 5. Baric dependences of the melting point (A and C) and its derivative with respect to pressure $T'_m(P)$ (B and D) for BCC and FCC-Fe in the pressure region 0−20 GPa (A and B), and 0−100 GPa (C and D). The triple points $\delta-\gamma$-liquid and $\gamma-\varepsilon$-liquid with coordinates from (24) and (25) are shown as solid dots. Our calculations for macro-Fe are shown as central solid lines, and for nano-Fe as dotted lines.

calculated results with the three-parameter Simon−Glatzel equation (21) in [72], the following parameters were obtained: $T_{m0} = 1822.88$ K, $P_0 = 32.51$ GPa, $c_s = 0.4644$ — lower dash-dotted line in Figure 5.

In [73] the dependence $T_m(P, \infty)$ for iron macrocrystal was also calculated by the analytical SMM method, but using the work-heat equivalence principle, i. e. SMM-WHEP. In [73] the dependence $T_m(P, \infty)$ was calculated for both BCC-Fe macrocrystal and the hexagonal phase ε-Fe. By approximating the calculated results with the three-parameter the Simon−Glatzel equation (21), the following parameters were obtained in [73]: for BCC-Fe: $T_{m0} = 1811$ K, $P_0 = 16.86$ GPa, $c_s = 1/2.38 = 0.42$ — solid upper line in Figure 5, for ε-Fe: $T_{m0} = 1811$ K, $P_0 = 16.88$ GPa, $c_s = 1/2.44 = 0.41$ — upper dashed-dotted line in Figure 5.

When using potential parameters (1) from the Table, using formulas (5)−(11) for BCC-Fe on the isotherm $T_m(0, \infty) = 1811$ K at $P = 0$ for the parameters included in formulas (14) and (15) we obtained

$$c_o\big(0, T_m(0), \infty\big) = 2.54003 \cdot 10^{-10}\,\text{m},$$

$$\Theta_o\big(0, T_m(0), \infty\big) = 372.609\,\text{K},$$

$$c_o\big(0, T_m(0), 281, 1\big) = 2.55123 \cdot 10^{-10}\,\text{m},$$

$$\Theta_o\big(0, T_m(0), 281, 1\big) = 340.166\,\text{K}.$$

For FCC-Fe on the isotherm $T_m(5.2\,\text{GPa}, \infty) = 1991$ K at $P = 5.2$ GPa for the parameters included in formulas (14) and (15) we obtained

$$c_o\big(0, T_m(5.2\,\text{GPa}), \infty\big) = 2.57718 \cdot 10^{-10}\,\text{m},$$

$$\Theta_o\big(0, T_m(5.2\,\text{GPa}), \infty\big) = 383.767\,\text{K},$$

$$c_o\big(0, T_m(5.2\,\text{GPa}), 306, 1\big) = 2.58242 \cdot 10^{-10}\,\text{m},$$

$$\Theta_o\big(0, T_m(5.2\,\text{GPa}), 306, 1\big) = 356.783\,\text{K}.$$

Our calculations for macrocrystal are shown by the central solid lines. The dotted lines show our calculations for cubic nanocrystal. In this scale our dependences $T_m(P, \infty)$ practically merge both with each other and with the experimental dependence from [65].

As can be seen from Figure 5, the dependence $T_m(P, N)$ for a nanocrystal lays lower than for macrocrystal, and the baric dependences of the functions $T'_m(P)$ for cubic macro- and nanocrystals do not have maximum as in the case of gold. However, as in the case of gold and platinum, the dependence of the function $T'_m(P)$ on size and shape for BCC and FCC-Fe is insignificant. This indicates that, with constant $N-f$-arguments the baric dependences $T_m(P, \infty)$ and $T_m(P, N, f)$ are practically parallel.

6. Conclusion

Within the RP-model the method is proposed for calculating the baric dependence of the melting point for nanocrystal consisting of N atoms, and which has the shape of rectangular parallelepiped with variable surface shape. It is shown that this method takes into account the dependence of the equation of state and other lattice properties on the size and shape of the nanocrystal.

Calculations of the dependence of the melting point on pressure P, size N and shape f of nanocrystal were carried out for FCC-Au, FCC-Pt, BCC and FCC-Fe. It is shown that at any pressure the melting point $T_m(P, N, f)$ decreases both with isomorphic-isobaric decrease in the number of atoms N and with isomer-isobaric deviation of the nanocrystal shape from the energy-optimal shape (for RP-models it is cube).

It is shown that the value of the baric derivative of the melting point $T'_m(P)$ for nanocrystal at low pressures is greater, and at high pressures it is less than the value $T'_m(P)$ for a macrocrystal. In this case, the dependence of the function $T'_m(P)$ on the size of the nanocrystal is insignificant, i. e., for constant $N-f$-arguments the baric dependences $T_m(P, \infty)$ and $T_m(P, N, f)$ are practically parallel.

It is known [74,75] that a nanocrystal embedded into a matrix of more refractory substance can be overheated above the melting point of the massive substance from which the nanocrystal consists, i. e., the following is observed: $T_m(P, N)^* = T_m(P, N, f)/T_m(P, \infty) > 1$. By measuring the value $T_m(P, N)^*$ and the number of atoms in the embedded nanocrystal, using our calculation method we can estimate the pressure under which the nanocrystal is located in the matrix.

Acknowledgments

The author expresses gratitude to S.P. Kramynin, K.N. Magomedov, Z.M. Surkhaeva, and N.Sh. Gazanova for fruitful discussions and assistance in study.

Conflict of interest

The author declares that he has no conflict of interest.

References

[1] N.R.C. Corsini, W.R. Little, A. Karatutlu, Y. Zhang, O. Ersoy, P.D. Haynes, C. Molteni, N.D.M. Hine, I. Hernandez, J. Gonzalez, F. Rodriguez, V.V. Brazhkin, A. Sapelkin. Nano Lett. **15**, *11*, 7334 (2015). https://doi.org/10.1021/acs.nanolett.5b02627.

[2] F. Bai, K. Bian, X. Huang, Z. Wang, H. Fan. Chem. Rev. **119**, *12*, 7673 (2019). https://doi.org/10.1021/acs.chemrev.9b00023.

[3] Y. Chen, Z. Lai, X. Zhang, Z. Fan, Q. He, C. Tan, H. Zhang. Nature Rev. Chem. **4**, *5*, 243 (2020). https://doi.org/10.1038/s41570-020-0173-4.

[4] T. Xiao, Y. Nagaoka, X. Wang, T. Jiang, D. Lamontagne, Q. Zhang, C. Cao, X. Diao, J. Qiu, Y. Lu, Z. Wang, Y.C. Cao. Science **377**, *6608*, 870 (2022). https://doi.org/10.1126/science.abq7684.

[5] I.M. Padilla Espinosa, T.D.B. Jacobs, A. Martini. Nanoscale Res. Lett. **17**, *1*, 96 (2022). https://doi.org/10.1186/s11671-022-03734-z.

[6] D. Vollath, F.D. Fischer, D. Holec. Beilstein J. Nanotechnology **9**, *1*, 2265 (2018). https://doi.org/10.3762/bjnano.9.211.

[7] X. Zhang, W. Li, H. Kou, J. Shao, Y. Deng, X. Zhang, J. Ma, Y. Li, X. Zhang. J. Appl. Phys. **125**, *18*, 185105 (2019). https://doi.org/10.1063/1.5090301.

[8] A. Forslund, A. Ruban. Phys. Rev. B **105**, *4*, 045403 (2022). https://doi.org/10.1103/PhysRevB.105.045403.

[9] A.S. Kholtobina, A. Forslund, A.V. Ruban, B. Johansson, N.V. Skorodumova. Phys. Rev. B **107**, *3*, 035407 (2023). https://doi.org/10.1103/PhysRevB.107.035407.

[10] S. Zhu, K. Xie, Q. Lin, R. Cao. Adv. Colloid Interface Sci. **315**, 102905 (2023). https://doi.org/10.1016/j.cis.2023.102905.

[11] M.N. Magomedov. FTT **64**, *7*, 765 (2022). (in Russian). https://doi.org/10.21883/FTT.2022.07.52559.319. [M.N. Magomedov. Phys. Solid State **64**, *7*, 765 (2022).] https://doi.org/10.21883/PSS.2022.07.54579.319].

[12] M.N. Magomedov. FTT **65**, *5*, 734 (2023). (in Russian). https://doi.org/10.21883/FTT.2023.05.55489.46. [M.N. Magomedov. Phys. Solid State **65**, *5*, 708 (2023). https://doi.org/10.21883/PSS.2023.05.56040.46].

[13] M.N. Magomedov. Crystallography Rep. **62**, *3*, 480 (2017). https://doi.org/10.1134/S1063774517030142.

[14] M.N. Magomedov. FTT **62**, *12*, 2034 (2020). (in Russian). https://doi.org/10.21883/FTT.2020.12.50206.172. [M.N. Magomedov. Phys. Solid State **62**, *12*, 2280 (2020). https://doi.org/10.1134/S1063783420120197].

[15] E.N. Ahmedov. J. Phys.: Conf. Ser. **1348**, *012002*, 1 (2019). https://doi.org/10.1088/1742-6596/1348/1/012002.

[16] S.P. Kramynin. Phys. Met. Metallography **123**, *2*, 107 (2022). https://doi.org/10.1134/S0031918X22020065.

[17] S.P. Kramynin. J. Phys. Chem. Solids **152**, 109964 (2021). https://doi.org/10.1016/j.jpcs.2021.109964.

[18] S.P. Kramynin. Solid State Sci. **124**, 106814 (2022). https://doi.org/10.1016/j.solidstatesciences.2022.106814.

[19] R. Briggs, F. Coppari, M.G. Gorman, R.F. Smith, S.J. Tracy, A.L. Coleman, A. Fernandez-Panella, M. Millot, J.H. Eggert, D.E. Fratanduono. Phys. Rev. Lett. **123**, *4*, 045701 (2019). https://doi.org/10.1103/PhysRevLett.123.045701.

[20] D.E. Fratanduono, M. Millot, D.G. Braun, S.J. Ali, A. Fernandez-Pañella, C.T. Seagle, J.-P. Davis, J.L. Brown, Y. Akahama, R.G. Kraus, M.C. Marshall, R.F. Smith,

E.F. O'Bannon III, J.M. Mcnaney, J.H. Eggert. Science **372**, *6546*, 1063 (2021). https://doi.org/10.1126/science.abh0364.
[21] T. Castro, R. Reifenberger, E. Choi, R.P. Andres. Phys.Rev. B **42**, *13*, 8548 (1990). https://doi.org/10.1103/PhysRevB.42.8548.
[22] M.N. Magomedov. FTT **63**, *9*, 1415 (2021). (in Russian). https://doi.org/10.21883/FTT.2021.09.51279.080. [M.N. Magomedov. Phys. Solid State **63**, *10*, 1465 (2021). https://doi.org/10.1134/S1063783421090250].
[23] G. Weck, V. Recoules, J.A. Queyroux, F. Datchi, J. Bouchet, S. Ninet, G. Garbarino, M. Mezouar, P. Loubeyre. Phys. Rev. B **101**, *1*, 014106 (2020). https://doi.org/10.1103/PhysRevB.101.014106.
[24] P. Cheyssac, R. Kofman, R. Garrigos. Phys. Scripta **38**, *2*, 164 (1988). https://doi.org/10.1088/0031-8949/38/2/009.
[25] R. Garrigos, P. Cheyssac, R. Kofman. Mol. Clusters **12**, *1–4*, 497 (1989). https://doi.org/10.1007/BF01427006.
[26] S.L. Lai, J.Y. Guo, V. Petrova, G. Ramanath, L.H. Allen. Phys. Rev. Lett. **77**, *1*, 99 (1996). https://doi.org/10.1103/PhysRevLett.77.99.
[27] G. Kellermann, A.F. Craievich. Phys. Rev. B **78**, *5*, 054106 (2008). https://doi.org/10.1103/physrevb.78.054106.
[28] T.S. Zhu, M. Li. Mater. Res. Bull. **63**, 253 (2015). https://doi.org/10.1016/j.materresbull.2014.12.010.
[29] F. Ercolessi, W. Andreoni, E. Tosatti. Phys. Rev. Lett. **66**, *7*, 911 (1991). https://doi.org/10.1103/physrevlett.66.911.
[30] F. Delogu. Phys. Rev. B **72**, *1*, 205418 (2005). https://doi.org/10.1103/PhysRevB.72.205418.
[31] M.N. Magomedov. Tech. Phys. **56**, *9*, 1277 (2011). https://doi.org/10.1134/S106378421109012X.
[32] M.N. Magomedov. Tech. Phys. **59**, *5*, 675 (2014). https://doi.org/10.1134/S1063784214050211.
[33] M.N. Magomedov. Tech. Phys. **61**, *5*, 730 (2016). https://doi.org/10.1134/S1063784216050157.
[34] M.N. Magomedov. J. Surface Investigation. X-ray, Synchrotron Neutron Techn. **13**, *5*, 880 (2019). https://doi.org/10.1134/S1027451019050070.
[35] L.A. Girifalco. Statistical Physics of Materials. J. Wiley and Sons Ltd., N.Y. (1973). 346 p.
[36] P.I. Dorogokupets, T.S. Sokolova, B.S. Danilov, K.D. Litasov. Geodynamics & Tectonophysics **3**, *2*, 129 (2012)]. https://doi.org/10.5800/GT-2012-3-2-0067.
[37] M. Mohr, A. Caron, P. Herbeck-Engel, R. Bennewitz, P. Gluche, K. Brühne, H.-J. Fecht. J. Appl. Phys. **116**, *12*, 124308 (2014). https://doi.org/10.1063/1.4896729.
[38] A. Rida, E. Rouhaud, A. Makke, M. Micoulaut, B. Mantisi. Phil. Mag. **97**, *27*, 2387 (2017). https://doi.org/10.1080/14786435.2017.1334136.
[39] M. Goyal, B.R.K. Gupta. Mod. Phys. Lett. B **33**, *26*, 1950310 (2019). https://doi.org/10.1142/s021798491950310x.
[40] J. Li, B. Lu, H. Zhou, C. Tian, Y. Xian, G. Hu, R. Xia. Phys. Lett. A **383**, *16*, 1922 (2019). https://doi.org/10.1016/j.physleta.2018.10.053.
[41] C.Q. Sun. Prog. Mater. Sci. **54**, *2*, 179 (2009). https://doi.org/10.1016/j.pmatsci.2008.08.001.
[42] I.F. Golovnev, E.I. Golovneva. Phys. Mesomech. **23**, *3*, 189 (2020). https://doi.org/10.1134/S1029959920030017.
[43] X. Wei, D.J. Shu. Phys. Rev. B **106**, *19*, 195419 (2022). https://doi.org/10.1103/PhysRevB.106.195419.
[44] M. Zhao, Y. Xia. Nature Rev. Mater. **5**, *6*, 440 (2020). https://doi.org/10.1038/s41578-020-0183-3.
[45] M.G. Pamato, I.G. Wood, D.P. Dobson, S.A. Hunt, L. Vočadlo. J. Appl. Crystallography **51**, *2*, 470 (2018). https://doi.org/10.1107/S1600576718002248.
[46] T. Tsuchiya. J. Geophys. Res. **108**, *B10*, 2462 (2003). https://doi.org/10.1029/2003JB002446.
[47] M. Zhu, J. Liu, Q. Huang, J. Dong, X. Yang. J. Phys. D **55**, *48*, 485303 (2022). https://doi.org/10.1088/1361-6463/ac9485.
[48] D. Errandonea. J. Appl. Phys. **108**, *3*, 033517 (2010). https://doi.org/10.1063/1.3468149.
[49] E.N. Ahmedov. Physica B: Condens. Matter **571**, 252 (2019). https://doi.org/10.1016/j.physb.2019.07.027.
[50] J. Chen, X. Fan, J. Liu, C. Gu, Y. Shi, D.J. Singh, W. Zheng. J. Phys. Chem. C **124**, *13*, 7414 (2020). https://doi.org/10.1021/acs.jpcc.9b10769.
[51] D. Shekhawat, M. Vauth, J. Pezoldt. Inorganics **10**, *4*, 56 (2022). https://doi.org/10.3390/inorganics10040056.
[52] D.M. Foster, T. Pavloudis, J. Kioseoglou, R.E. Palmer. Nature Commun. **10**, *1*, 2583 (2019). https://doi.org/10.1038/s41467-019-10713-z.
[53] C. Zeni, K. Rossi, T. Pavloudis, J. Kioseoglou, S. de Gironcoli, R.E. Palmer, F. Baletto. Nature Commun. **12**, *1*, 6056 (2021). https://doi.org/10.1038/s41467-021-26199-7.
[54] M.N. Magomedov. Phys. Solid State **46**, *5*, 954 (2004). https://doi.org/10.1134/1.1744976.
[55] D. Errandonea. Phys. Rev. B **87**, *5*, 054108 (2013). https://doi.org/10.1103/PhysRevB.87.054108.
[56] N.N. Patel, M. Sunder. High pressure melting curve of platinum up to 35 GPa. AIP Conf. Proc. AIP Publishing LLC **1942**, *1*, 030007 (2018). https://doi.org/10.1063/1.5028588.
[57] S. Anzellini, V. Monteseguro, E. Bandiello, A. Dewaele, L. Burakovsky, D. Errandonea. Sci. Rep. **9**, *13034*, 1 (2019). https://doi.org/10.1038/s41598-019-49676-y.
[58] Z.M. Geballe, N. Holtgrewe, A. Karandikar, E. Greenberg, V.B. Prakapenka, A.F. Goncharov. Phys. Rev. Mater. **5**, *3*, 033803 (2021). https://doi.org/10.1103/PhysRevMaterials.5.033803.
[59] V.M. Samsonov, A.A. Romanov, A.Y. Kartoshkin, I.V. Talyzin, V.V. Puytov. Appl. Phys. A **128**, *9*, 826 (2022). https://doi.org/10.1007/s00339-022-05922-1.
[60] E. Toulkeridou, J. Kioseoglou, P. Grammatikopoulos. Nanoscale Adv. **4**, *22*, 4819 (2022). https://doi.org/10.1039/d2na00418f.
[61] H.M. Strong, R.E. Tuft, R.E. Hanneman. Metallurgical Trans-act. **4**, 2657 (1973). https://doi.org/10.1007/BF02644272.
[62] L.J. Swartzendruber. Bull. Alloy Phase Diagrams **3**, *2*, 161 (1982). https://doi.org/10.1007/BF02892374.
[63] Q. Williams, R. Jeanloz, J. Bass, B. Svendsen, T.J. Ahrens. Science **236**, *4798*, 181 (1987). https://doi.org/10.1126/science.236.4798.181.
[64] R. Boehler. Nature **363**, *6429*, 534 (1993). https://doi.org/10.1038/363534a0.
[65] S. Anzellini, A. Dewaele, M. Mezouar, P. Loubeyre, G. Morard. Science **340**, *6131*, 464 (2013). https://doi.org/10.1126/science.1233514.
[66] P.I. Dorogokupets, A.M. Dymshits, K.D. Litasov, T.S. Sokolova. Sci. Rep. **7**, *1*, 1 (2017). https://doi.org/10.1038/srep41863.
[67] I.C. Ezenwa, Y. Fei. Geophys. Res. Lett. **50**, *6*, e2022GL102006 (2023). https://doi.org/10.1029/2022GL102006.

[68] M.N. Magomedov. Phys. Solid State **63**, *2*, 215 (2021). https://doi.org/10.1134/S1063783421020165.
[69] M.N. Magomedov. J. Phys. Chem. Solids **151**, 109905 (2021). https://doi.org/10.1016/j.jpcs.2020.109905.
[70] M.N. Magomedov. Phys. Solid State **64**, *13*, 2121 (2022). https://doi.org/10.21883/PSS.2022.13.52307.145.
[71] M.N. Magomedov. ZhTF **93**, *2*, 221 (2023). (in Russian). https://doi.org/10.21883/JTF.2023.02.54496.190-22.
[M.N. Magomedov. Tech. Phys. **68**, *2*, 209 (2023). https://doi.org/10.21883/TP.2023.02.55474.190-22].
[72] T.D. Cuong, A.D. Phan. Vacuum **185**, 110001 (2021). https://doi.org/10.1016/j.vacuum.2020.110001.
[73] T.D. Cuong, N.Q. Hoc, N.D. Trung, N.T. Thao, A.D. Phan. Phys. Rev. B **106**, *9*, 094103 (2022). https://doi.org/10.1103/PhysRevB.106.094103.
[74] W.H. Qi, M.P. Wang. Mater. Lett. **59**, *18*, 2262 (2005). https://doi.org/10.1016/j.matlet.2004.06.079.
[75] M.A. Jabbareh. Solid State Commun. **355**, 114923 (2022). https://doi.org/10.1016/j.ssc.2022.114923.

Translated by I.Mazurov